Mathematical Model for the Hemodynamic Response to Venous Occlusion Measured With Near-Infrared Spectroscopy in the Human Forearm

Article *in* IEEE transactions on bio-medical engineering · April 2007

DOI: 10.1109/TBME.2006.890123 · Source: PubMed

CITATIONS
26

READS
298

5 authors, including:

Toi Van Vo
International University of Vietnam National Universities, Ho Chi Minh City
285 PUBLICATIONS **3,207** CITATIONS
SEE PROFILE

Peter E. Hammer
Harvard Medical School
97 PUBLICATIONS **1,840** CITATIONS
SEE PROFILE

Shalini Nadgir
University of Colorado Colorado Springs
7 PUBLICATIONS **218** CITATIONS
SEE PROFILE

Sergio Fantini
Tufts University
421 PUBLICATIONS **9,919** CITATIONS
SEE PROFILE

Mathematical Model for the Hemodynamic Response to Venous Occlusion Measured With Near-Infrared Spectroscopy in the Human Forearm

Toi Van Vo, Peter E. Hammer, Matthew L. Hoimes, Shalini Nadgir, and Sergio Fantini*

***Abstract*—We propose a mathematical model to describe the hemodynamic changes induced by a venous occlusion in a human limb. These hemodynamic changes, which include an increase in blood volume, a reduction in blood flow, and modifications to the oxygen saturation of hemoglobin, can all be measured noninvasively with near-infrared spectroscopy (NIRS). To test the model, we have performed NIRS measurements on the human forearm, specifically on the brachioradialis muscle, during venous occlusion induced by a pneumatic cuff inflated around the upper arm to pressures within the range 10–60 mmHg. We have found a good agreement between parameters measured by NIRS (total hemoglobin concentration and hemoglobin saturation) and the corresponding model parameters (capacitor voltage and arterial/capillary branch current). In particular, model and experiment indicate that the time constant for blood accumulation during venous occlusion (∼73–79 s) is much slower than the time constant for blood drainage following cuff release (∼5 s). These results indicate that this mathematical model can be a valuable analytical tool to characterize, optimize, and further develop diagnostic measurement schemes that use venous occlusion approaches.**

***Index Terms*—Blood flow, hemoglobin concentration, hemoglobin saturation, mathematical model, near-infrared spectroscopy, venous occlusion.**

I. Introduction

MATHEMATICAL models have been commonly proposed to study and describe the vascular system. Windkessel models, for example, use electrical resistors to represent vascular resistance, capacitors to represent the compliance, and inductors to represent the inertance. They are based on hemodynamic principles and have become the most widely used lumped models to investigate pressures and flows of systemic circulation [1]–[3]. In the investigation of circulatory assistance, mathematical models have been developed in which the heart and blood vessels are represented by resistive-capacitive networks, pressures and pressure gradients by voltages, blood flow by electric current, and cardiac valves by diodes [4]–[6]. In particular, a time-varying capacitance in series with a resistance was used to model pressure and flow at the outlet of a ventricle [7], whereas a network of resistors and capacitors have been used to model postocclusive reactive hyperemia in extremities [8].

Near-infrared spectroscopy (NIRS) is a noninvasive technique for the functional and metabolic study of tissue. The absorption of near-infrared light in tissue is mainly due to hemoglobin in its oxygenated ($\mathrm{HbO_2}$) and deoxygenated (Hb) forms. Spectral measurements allow for the separate determination of the concentrations of these two species ($[\mathrm{HbO_2}]$ and [Hb]) in tissue, which lead to the total hemoglobin concentration ($\mathrm{THC} = [\mathrm{HbO_2}] + [\mathrm{Hb}]$) and hemoglobin saturation ($\mathrm{StO_2} = [\mathrm{HbO_2}]/\mathrm{THC}$). THC and $\mathrm{StO_2}$ are indicative of the balance between the local blood flow, blood volume, and oxygen utilization rate, which are relevant physiological and metabolic parameters. NIRS has been widely applied to skeletal muscles *in vivo* to investigate the oxygenation and blood volume changes induced by vascular occlusion. During the ischemic response caused by arterial occlusion, the initial rate of decrease of $[\mathrm{HbO_2}]$ is equal to the initial rate of increase of [Hb], resulting in a constant THC (i.e., constant blood volume) and a decrease in blood oxygenation [9]. The rate of decrease in blood oxygenation during arterial occlusion, i.e. in the absence of blood flow, provides a measure of the tissue oxygen consumption [9], [10]. During venous occlusion, while the arterial inflow is initially unaffected, the venous return is blocked, so that the THC shows an initial increase as a direct result of blood accumulation [11]. The initial rate of increase in THC during venous occlusion yields a measure of the blood flow [11]. Under the hypothesis that this initial increase in THC results from the accumulation of venous blood, it has been proposed that one can translate the individual increases in $[\mathrm{HbO_2}]$ and [Hb] into a measurement of the venous saturation [12], [13]. These results show that vascular occlusions induce hemodynamic changes that allow for noninvasive, optical measurements of a number of physiologically important parameters. In particular, venous occlusions are ideally suited to clinical applications as a result of their lack of discomfort as opposed to the stronger pressures associated with arterial occlusions.

Manuscript received July 2, 2006; revised September 16, 2006. This work was supported in part by the National Science Foundation (NSF) under Grant BES-93840. *Asterisk indicates corresponding author.*

T. V. Vo, M. L. Hoimes, and S. Nadgir are with the Department of Biomedical Engineering, Tufts University, Medford, MA 02155 USA.

P. E. Hammer is with the Department of Biomedical Engineering, Tufts University, Medford, MA 02155 USA and also with the Departments of Cardiac Surgery and Anesthesiology, Children's Hospital Boston, Boston, MA 02115 USA.

*S. Fantini is with the Department of Biomedical Engineering, Tufts University, Medford, MA 02155 USA (e-mail: sergio.fantini@tufts.edu).

Color versions of one or more of the figures in this paper are available online at http://ieeexplore.ieee.org.

Digital Object Identifier 10.1109/TBME.2006.890123

Vascular occlusions are commonly achieved by applying a pneumatic cuff to the limb, and by inflating the cuff to a given pressure (>200 mmHg for arterial occlusion, and in the range 40–60 mmHg for venous occlusion). In a study on the effect of the cuff pressure and speed of inflation on the measurement of blood flow and oxygen consumption, NIRS measurements were performed on human calf muscles while applying different pressures to a pneumatic cuff placed around the thigh of the subject [14]. It was found that when the cuff pressure reaches a threshold value (about 30 mmHg) the venous outflow is hindered and when it reaches a critical value (between 30 and 45 mmHg) a complete venous occlusion occurs. Furthermore, if the pressure increases from 30 mmHg to 45 mmHg in less than about 6 s, the blood flow and oxygen consumption measured according to the venous-occlusion protocol [11] were independent of the inflation time and final cuff pressure [14].

In this work, we have modeled the vascular system with an electrical circuit to describe the hemodynamic response induced by an externally applied pressure. To test and validate our model, we have experimentally investigated the variations in THC and StO_2 in the human forearm in response to an external pressure in the range 10–60 mmHg applied by a pneumatic cuff around the upper arm. The development of a model specifically aimed at describing the response of hemodynamic parameters measured with near-infrared spectroscopy to venous occlusion can help optimize measurement protocols and identify new approaches to the noninvasive measurement of functional and metabolic parameters.

II. Methods

A. The External Pressure as Added Resistance: Variable Resistor Model

A first circuit model that we propose to describe the hemodynamic response to venous occlusion is shown in Fig. 1(a). This model applies to vascular occlusions that mostly affect the veins and minimally perturb the arteries, which is the case if the externally applied cuff pressure is below the arterial blood pressure. In this model, every circuit element has a direct correspondence to a physiological or vascular parameter. The constant voltage sources V_a and V_v represent mean arterial pressure (MAP) and central venous pressure (CVP), respectively. The resistor R_a represents the resistance to blood flow between the large arteries of the upper arm and the forearm veins. The capacitor C represents the compliance of the forearm veins; compliance of the forearm arteries is neglected because the factors that comprise it, distensibility and total volume, are about 1/7 and 1/4, respectively, of the corresponding values for the veins [15]. The resistor R_{v1} represents the resistance to blood flow between the small veins of the forearm and the upper arm veins that drain the forearm (i.e., the cephalic and basilic veins). The variable resistor R_{v2} represents the resistance to blood flow in the portion of the cephalic and basilic veins encircled by the cuff, and is the critical element of the model as it represents the effect of the external cuff pressure. This is a variable resistor because its value changes with the difference between the cuff pressure and the blood pressure in the large veins of the forearm. This pressure difference will be referred to here as transmural pressure, P_t. The total steady-state resistance to blood flow in the forearm can be expressed as follows:

$$R_{tot} = \frac{\text{MAP} - \text{CVP}}{\frac{\text{FBF}}{60} \times 10 \times FTV}, \tag{1}$$

where units for resistance are mmHg/(ml/s), FBF is forearm blood flow in ml/min/100 ml tissue, and FTV is forearm tissue volume in liters. The values of R_a and R_{v1} are treated as constants and are computed as fixed percentages of R_{tot} based on typical pressure drops across the various types of vessels comprising systemic vascular beds (e.g., arteries, arterioles, capillaries, venules and veins). The complexity of this apparently straightforward model lies in finding the relationship between R_{v2} and the externally applied pressure. Here is how we proceed.

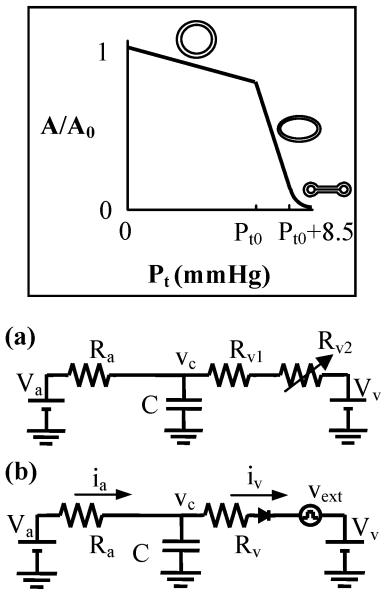

Fig. 1. (a) Variable resistor model for the hemodynamic changes induced by venous occlusion. The voltage sources V_a and V_v model the arterial and venous pressures, respectively. The vascular resistance is modeled by resistors R_a, R_{v1} and R_{v2} while the effect of venous compliance is modeled by capacitor C. Resistor R_{v2} is a variable resistor whose value is directly dependent on the externally applied pressure. (b) Voltage-source/diode model for the hemodynamic changes induced by venous occlusion. The voltage sources V_a and V_v model the arterial and venous pressures, respectively, and v_{ext}, in combination with the diode, represents the influence of cuff pressure. The currents i_a and i_v represent the arterial/capillary and venous blood flow, respectively. The vascular resistance is modeled by resistors R_a and R_v, while the effect of venous compliance is modeled by capacitor C. The ideal diode imposes that i_v never flows in the direction opposite to that indicated by the arrow. (Inset) Modeled relationship between the normalized cross-sectional area of a large vein (A/A_0) and the vascular transmural pressure (P_t) during limb compression by a cuff [16]. We have approximated data from the original study of [16] by three piece-wise fits representing three distinct regimes of vessel behavior. For P_t between zero and P_{t0}, the vein maintains a circular shape as it is compressed, and its area decreases linearly with P_t. For P_t between P_{t0} and $P_{t0} + 8.5$ mmHg, the vein becomes elliptical in cross-section with increasing eccentricity, and this segment was also fit by a line. For P_t greater than $P_{t0} + 8.5$ mmHg, the vein is assumed to be collapsed so that opposite walls are in contact for part of their length and only a circular area at each end of this line of contact remains open. This portion of the curve was fit by an exponential function. See text for details.

TABLE I
MODEL PARAMETERS

Parameter	Value	Units	Notes
MAP	100	mmHg	(typ)
CVP	5	mmHg	(typ)
FBF	3	ml/min/100 ml tissue	Ref. [21]
FTV	1.8	liters	(typ)
R_a	99	mmHg/(ml/s)	Calculated by scaling R_{total} by the proportion of pressure that is lost across arteries, arterioles and capillaries of a typical vascular bed [15].
R_{v1}	7	mmHg/(ml/s)	Calculated by scaling R_{total} by the proportion of pressure that is lost across venules and veins of a typical vascular bed [15].
C	0.8	ml/mmHg	Calculated by scaling the compliance of both arms, from Ref. [22], based on the relative volume of veins in a single forearm.
η	5e-5	mmHg sec	Ref. [15]
L	5	cm	(typ)
r_0	0.2	cm	(typ)
P_{t0}	5	mmHg	(see text)

For negative values of the transmural pressure P_t (i.e. when the inside pressure is greater than the outside pressure for a blood vessel), we first express the volume of the vein segment affected by the external pressure, V_{seg}, as a function of P_t as follows:

$$V_{\text{seg}} = C_{\text{seg}} P_t + (V_u)_{\text{seg}} \tag{2}$$

where C_{seg} is the compliance of the venous segment and $(V_u)_{\text{seg}}$ is its unstressed volume, computed as $\pi r_u^2 L$, with r_u and L the unstressed radius and the length, respectively, of the segment. The resistance of this segment can then be computed using Poiseuille's Law

$$R_{\text{seg}} = \frac{8\eta L}{\pi r_{\text{seg}}^4} \tag{3}$$

where $r_{\text{seg}} = \sqrt{V_{\text{seg}}/(\pi L)}$ and η is the viscosity of blood.

For positive values of P_t, we have considered a study by Dai *et al.* [16] to determine the relationship between P_t and the cross-sectional area (A) of a large vein during circumferentially symmetric limb compression by a cuff. We approximated the data reported by Dai *et al.* [16] by three piece-wise fits representing three distinct regimes of vessel behavior, as shown in Fig. 1 (inset).

For P_t between zero and a given value P_{t0}, the vein maintains a circular shape as it is compressed. The value of P_{t0} corresponding to the results of Dai *et al.* [16] is approximately 35 mmHg. This portion of the curve (i.e. $0 \le P_t < P_{t0}$) is fit by the straight line $A/A_0 = 1 - 0.2208\, P_t/P_{t0}$, where A_0 is the cross-sectional area at zero transmural pressure. In this initial regime, the radius of the compressed venous segment is computed as $r_{\text{seg}} = r_u\sqrt{A/A_0}$, and Poiseuille's Law (3) is used again to compute resistance.

For P_t between P_{t0} and $P_{t0} + 8.5\ \text{mmHg}$, the vein becomes elliptical in cross-section with increasing eccentricity. This segment is fit by the straight line $A/A_0 = -0.0709(P_t + P_{t0}) + 5.67$. The area of the ellipse is computed as the product of A/A_0 and $(A_u)_{\text{seg}}$, and the circumference of the ellipse is assumed to be constant and equal to the circular circumference just prior to elliptical deformation [17]. The major and minor semi-axes of the ellipse, a and b, can then be computed by simultaneously solving the equations for ellipse area and circumference in terms of a and b. The circumference equation does not have a closed-form solution, so we have used an approximation proposed by Ramanujan [18]. The two equations cannot be directly solved for a and b, so they were solved iteratively using the secant method with a convergence criterion $\varepsilon_2 = 10^{-5}$ [19]. Also in this second regime, the resistance is computed by Poiseuille's Law of (3), modified for a cylinder of elliptical cross-section [20] and expressed in terms of a and b.

For transmural pressures greater than $P_{t0} + 8.5\ \text{mmHg}$, the vein is assumed to be collapsed so that opposite walls are in contact for part of their length and only a circular area at each end of this line of contact remains open. We fit this portion of the curve by the exponential

$$\frac{A}{A_0} = 0.1777\, e^{-0.399(P_t - P_{t0} - 8.5\ \text{mmHg})} \tag{4}$$

where the constants were determined so that the curve and its derivative are continuous with the adjacent linear segment. Resistance was computed in the same way as for the case of P_t between zero and P_{t0} mmHg, except that the final resistance was calculated as the equivalent resistance of the two cylindrical regions in parallel.

All of the resistance calculations above were for a single segment of vein encircled by the cuff, so total resistance to blood leaving the forearm was computed as the parallel combination of two identical venous segments, representing the basilic vein and the cephalic vein, compressed in the same manner. The differential equation describing the mathematical model cannot be solved analytically because R_{v2} is a function of cuff pressure and intravascular (venous) pressure, so it was integrated numerically using a fourth-order Runge–Kutta algorithm [19] with step size of 0.01 s. Values of model parameters used for this numerical solution are reported in Table I. Note that the value of P_{t0} used for our simulations was lower than in the study by Dai *et al.* [16]. Their results of $P_{t0} \sim 35\ \text{mmHg}$ and vein collapse at $P_t \sim 43.5\ \text{mmHg}$ correspond to a deep leg vein and agree with

TABLE II
ANALYTICAL EXPRESSIONS FOR THE VOLTAGE-SOURCE/DIODE CIRCUIT MODEL FOR "SMALL" $V_{\rm ext}\,(V_{\rm ext} < V_{\rm crit})$

	$t < t_1$	$t_1 \le t < t_2$	$t \ge t_2$
$i_a(t)$	$I_a^{(\rm rest)}$	$\left[I_a^{(\rm rest)} - I_a^{(\rm occl)}\right]e^{-(t-t_1)/\tau_1} + I_a^{(\rm occl)}$	$\left[i_a(t_2^-) - I_a^{(\rm rest)}\right]e^{-(t-t_2)/\tau_1} + I_a^{(\rm rest)}$
$i_v(t)$	$I_v^{(\rm rest)}$	$\left[I_v^{(\rm rest)} - \frac{V_{\rm ext}}{R_v} - I_v^{(\rm occl)}\right]e^{-(t-t_1)/\tau_1} + I_v^{(\rm occl)}$	$\left[i_v(t_2^-) + \frac{V_{\rm ext}}{R_v} - I_v^{(\rm rest)}\right]e^{-(t-t_2)/\tau_1} + I_v^{(\rm rest)}$
$v_C(t)$	$V_a - R_a I_a^{(\rm rest)}$	$R_a\left[I_a^{(\rm occl)} - I_a^{(\rm rest)}\right]e^{-(t-t_1)/\tau_1} + V_a - R_a I_a^{(\rm occl)}$	$\left[v_C(t_2^-) - V_a + R_a I_a^{(\rm rest)}\right]e^{-(t-t_2)/\tau_1} + V_a - R_a I_a^{(\rm rest)}$

TABLE III
ANALYTICAL EXPRESSIONS FOR THE VOLTAGE-SOURCE/DIODE CIRCUIT MODEL FOR "LARGE" $V_{\rm ext}\,(V_{\rm ext} \ge V_{\rm crit})$

	$t < t_1$	$t_1 \le t < t^*$	$t^* \le t < t_2$	$t \ge t_2$
$i_a(t)$	$I_a^{(\rm rest)}$	$I_a^{(\rm rest)}e^{-(t-t_1)/\tau_2}$	$\left[i_a(t^{*-}) - I_a^{(\rm occl)}\right]e^{-(t-t^*)/\tau_1} + I_a^{(\rm occl)}$	$\left[i_a(t_2^-) - I_a^{(\rm rest)}\right]e^{-(t-t_2)/\tau_1} + I_a^{(\rm rest)}$
$i_v(t)$	$I_v^{(\rm rest)}$	0	$-I_v^{(\rm occl)}e^{-(t-t^*)/\tau_1} + I_v^{(\rm occl)}$	$\left[i_v(t_2^-) + \frac{V_{\rm ext}}{R_v} - I_v^{(\rm rest)}\right]e^{-(t-t_2)/\tau_1} + I_v^{(\rm rest)}$
$v_C(t)$	$V_a - R_a I_a^{(\rm rest)}$	$-R_a I_a^{(\rm rest)}e^{-(t-t_1)/\tau_2} + V_a$	$\left[v_C(t^{*-}) - V_a + R_a I_a^{(\rm occl)}\right]e^{-(t-t^*)/\tau_1} + V_a - R_a I_a^{(\rm occl)}$	$\left[v_C(t_2^-) - V_a + R_a I_a^{(\rm rest)}\right]e^{-(t-t_2)/\tau_1} + V_a - R_a I_a^{(\rm rest)}$

the threshold and critical pressure values of ∼30 mmHg and ∼30–45 mmHg, respectively, reported in a previous near-infrared spectroscopy study of venous occlusion in human legs [14]. This study considers more superficial arm veins, for which we have observed a value of $P_{t0} \sim 5\ \rm mmHg$, consistent with (A) studies on excised vein segments that have reported eccentric compression at transmural pressures between 0 and 1 mmHg [17], and (B) the assumption that the surrounding tissue of the arm provides some support but much less than that provided by the large leg muscles for deep leg veins.

B. External Pressure as a Voltage Source in Series With a Diode: Voltage-Source/Diode Model

While the model presented above represents a quantitative description of forearm hemodynamics during arm cuff inflation, it is rather complex, with many parameters needed to express R_{v2} in terms of P_t, and no analytical solution. We have developed a simpler model [shown in Fig. 1(b)], where the effect of the external pressure is described by a voltage source and a diode instead of the variable resistor of Fig. 1(a). While these circuit elements less closely resemble the physical mechanisms underlying the changes due to cuff inflation, they capture the essential dynamics with a much simpler model that allows for an analytical solution. The resistors R_a and R_v represent the same quantities as in the variable resistor model presented above (here, R_v represents the sum of R_{v1} and R_{v2} with no applied cuff pressure). The ideal diode D guarantees the unidirectional flow of i_v, the current through R_v, thus confining the effect of $v_{\rm ext}$ to limiting the amplitude of i_v without possibly changing its sign. The capacitor C, again, represents venous compliance, and the charge stored in the capacitor is specifically used to model the local blood volume. The time-dependent voltage source $v_{\rm ext}$ represents the overall effect of the pressure externally applied by the pneumatic cuff. The purpose of the voltage source here is to influence current (representing blood flow) by reducing the pressure gradient between the arteries and veins. To determine how $V_{\rm ext}$, the magnitude of the step in $v_{\rm ext}$, in the voltage source model relates to $P_{\rm cuff}$ in the variable resistor model, we found the value of $V_{\rm ext}$ that resulted in the same steady-state levels of i_a, i_v, and v_c as for a given value of $P_{\rm cuff}$. This was repeated for a range of values of $P_{\rm cuff}$, and we found that $V_{\rm ext}$ is related to $P_{\rm cuff}$ according to the simple translation: $V_{\rm ext} = P_{\rm cuff} - 22\ \rm mmHg$.

The analysis of the circuit model of Fig. 1(b) is straightforward, and the analytical solutions for the time dependence of the various parameters in response to a rectangular wave for $v_{\rm ext}$ are reported in the Appendix and Tables II and III for reference. The responses of this simplified, voltage source model and of the variable resistor model to a "small" rectangular wave of cuff pressure (i.e., $V_{\rm ext} < V_{\rm crit}$ where $V_{\rm crit} = (V_a - V_v)R_v/(R_a + R_v)$) are shown in Fig. 2(a). The critical voltage, $V_{\rm crit}$, is the minimum voltage that reverse-biases the diode and represents the minimum cuff pressure to achieve complete venous occlusion. The variable resistor model responses are based on numerical simulations, and the voltage source model responses are based on the analytical solution reported in the Appendix. When $v_{\rm ext}$ is suddenly increased, the current i_v suddenly jumps to a lower value due to the immediate effect of the cuff on blood flow drained from the forearm. This causes blood to accumulate in the veins of the forearm as seen in the comparatively gradual rise in v_c. As v_c rises, the voltage gradient forcing i_a decreases, so i_a also decreases mirroring the rise in v_c. When the cuff is released, forearm venous outflow jumps to a higher level due to the jump in gradient $(v_c - v_{\rm ext})$ then decays to the level of flow that preceded cuff inflation after the excess blood that had been stored in the forearm has been discharged through the arm veins. For "small" step sizes, the current through the diode is always greater than zero, so the dynamics are governed by the capacitor and the parallel combination of the arterial and venous resistances. The voltage source and variable resistor models achieve nearly identical steady-state values (both with the cuff fully inflated and fully deflated), and the transient response following cuff deflation is also very similar. Their responses only differ transiently following cuff inflation, where the voltage source

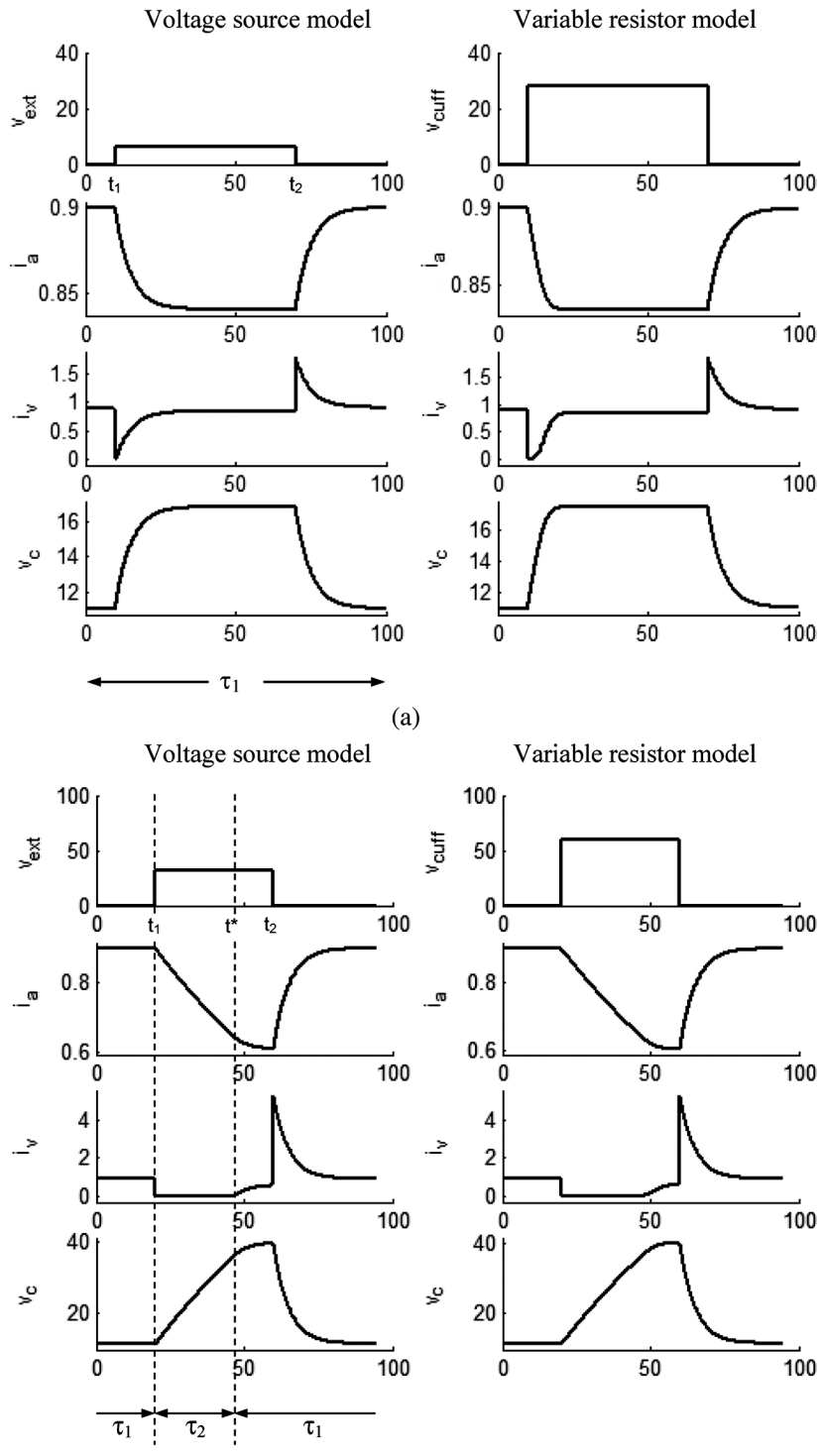

Fig. 2. Time dependence of three key model parameters (i_a, i_v, and v_c) in response to a rectangular voltage signal for the voltage source model and for the variable resistor model. Units on horizontal axes are time in seconds, and units on vertical axes are, from top to bottom, mmHg, ml/s, ml/s and mmHg. (a) Refers to the "small" $V_{\rm ext}$ case where the diode of Fig. 1(b) is always conducting and the circuit is characterized by a single time constant τ_1. (b) Refers to the "large" $V_{\rm ext}$ case where the diode of the voltage source model is nonconducting between times t and t^*, thus introducing a second circuit time constant, τ_2. The values of the model parameters are listed in Table I.

model responses follow simple first-order exponential behavior (fixed resistance–capacitance time constant) while the variable resistor model responses show the effect of the variable resistor and corresponding variable time constant.

The responses to a "large" rectangular wave of cuff pressure ($V_{\rm ext} > V_{\rm crit}$) are shown in Fig. 2(b). The main difference between these responses and those of Fig. 2(a) is that the "large" step size causes reverse biasing of the diode in the voltage source model (and, for the variable resistor model, a huge increase in the value of the variable resistor) with the effect of removing the low resistance (venous) branch from the equivalent resistance through which the capacitor charges and discharges. Note that

this effect only persists until the capacitor voltage rises to the point of forward biasing the diode (or decreasing the value of the variable resistor). For the case of the "large" step, both the steady-state and transient behavior of the two models are nearly indistinguishable.

An important feature of the voltage source model is that while for small V_{ext} this capacitive circuit has only one time constant (τ_1), for larger values of V_{ext} a second time constant $(\tau_2 > \tau_1)$ characterizes the circuit from the time t_1 at which the cuff pressure is applied to the time t^* at which the capacitor voltage v_c reaches a value of $V_v + V_{\text{ext}}$. The expressions for τ_1, τ_2, and t^* in terms of the circuit elements R_a, R_v, C and V_{ext} are reported in the Appendix. Typical values of model parameters (those used for the plots of Fig. 2 and listed in Table I) result in values of τ_1 and τ_2 of 5 s and 79 s, respectively. This corresponds to a time constant of forearm filling during large cuff pressures that is approximately 16 times that of forearm filling during small cuff pressures and that of forearm emptying.

Because the simplified model based on the voltage-source/diode combination is conceptually much simpler and has far fewer parameters than the variable resistor model, it is preferable to use it to simulate and fit NIRS data, given that the two models respond very similarly to rectangular pulses in cuff pressure. The only noticeable difference of the two models is during forearm filling resulting from a "small" cuff pressure step. Whether this difference is significant depends on the use of the model. For this study, where the signal-to-noise ratio of the NIRS measurements is not sufficient to discriminate such subtle differences between the models, we have used the much less complex voltage source model to fit and interpret the experimental NIRS data.

C. Experimental Setup for Near-Infrared Spectroscopy

To validate our model, we have performed optical measurements, in the human forearm, of the hemodynamic response to vascular occlusions. The optical instrument is a frequency-domain tissue spectrometer (OxiplexTS, ISS, Inc., Champaign, IL). For this study, we have used eight multiplexed, intensity-modulated laser diodes (four emitting at 690 nm and four at 830 nm) and one heterodyned photo-multiplier tube detector (PMT). The modulation frequency of the laser intensity is 110 MHz, the cross-correlation frequency for heterodyne detection is 5 kHz, and the multiplexing frequency of the eight lasers (to time share the optical detector) is 100 Hz. We averaged the data acquisition over fifteen multiplexing cycles of the eight light sources (each light source is on for $(100\ \text{Hz})^{-1} = 10\ \text{ms}$, so that one cycle through the eight light sources takes 80 ms), resulting in an overall acquisition time per data point of 1.2 s. The eight laser diodes and the PMT are all coupled to optical fibers. The optical probe used in this study arranges the eight illumination optical fibers (400 μm in core diameter) and one collection optical fiber (a fiber bundle with active diameter of 3 mm) over a four-distance linear array that is suitable for muscle studies. The four distances between the collection fiber and the four pairs of illumination fibers (each pair consisting of illumination fibers at 690 and 830 nm) are 2.0, 2.5, 3.0 and 3.5 cm. This multi-distance scheme allows for

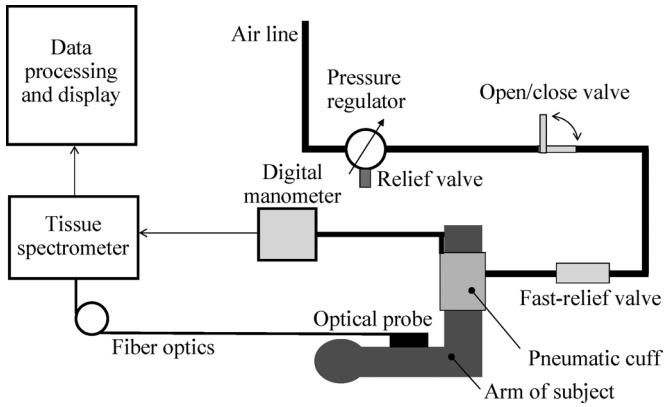

Fig. 3. Experimental setup for the optical measurement of hemodynamic changes in the human forearm induced by cuff-induced venous occlusions in the upper arm.

absolute measurements of the absorption and reduced scattering coefficients of tissue [23]. In turn, the measurements of absorption coefficients of tissue at two wavelengths are translated into measurements of hemoglobin-related parameters such as the THC and the StO_2 in tissue. THC is defined as the sum of the tissue concentrations of oxy-hemoglobin and deoxy-hemoglobin, while StO_2 is the oxygen saturation of hemoglobin (the ratio of oxy-hemoglobin to THC). THC is modeled by the capacitor charge $q = Cv_c$ in the circuits of Fig. 1. The oxygen saturation of hemoglobin in tissue (StO_2) is a balance between the oxygenation of arterial blood, the blood flow, and the tissue oxygen consumption. In the case considered here, namely a venous occlusion under rest conditions, the arterial blood oxygenation and the tissue oxygen consumption do not change significantly. Under these conditions, a hemodynamic model that we have previously reported [24] yields an expression for the change in tissue saturation (ΔStO_2) that for small changes in blood flow is proportional to the change in the speed of blood flow. To a first approximation, we assume that the change in the speed of blood flow is proportional to the change in the arterial/capillary current represented here by i_a. As a result, in the models of Fig. 1, we will consider changes in the arterial/capillary branch current (Δi_a) to be proportional to changes in the tissue saturation (ΔStO_2).

The optical probe was secured on the subject's forearm, over the brachioradialis muscle, while a pneumatic cuff was placed around the subject's upper arm. The cuff was inflated through a pressurized air line, and the cuff pressure was accurately controlled by a regulator (Fairchild Industrial Products Company, Winston-Salem, NC; Part no. 10222) that could be set to a specific pressure value (see the experimental setup in Fig. 3). By avoiding manual inflation, we were able to accurately set the final cuff pressure ($\leq$60 mmHg in this study) and reproducibly control the inflation rate. A pressure monitor (PM015D, World Precision Instruments, Inc., Sarasota, FL) permitted a digital read-out of the cuff pressure, and generated an analog output, which was fed to an auxiliary input port of the tissue spectrometer to record pressure values synchronously with near-infrared data.

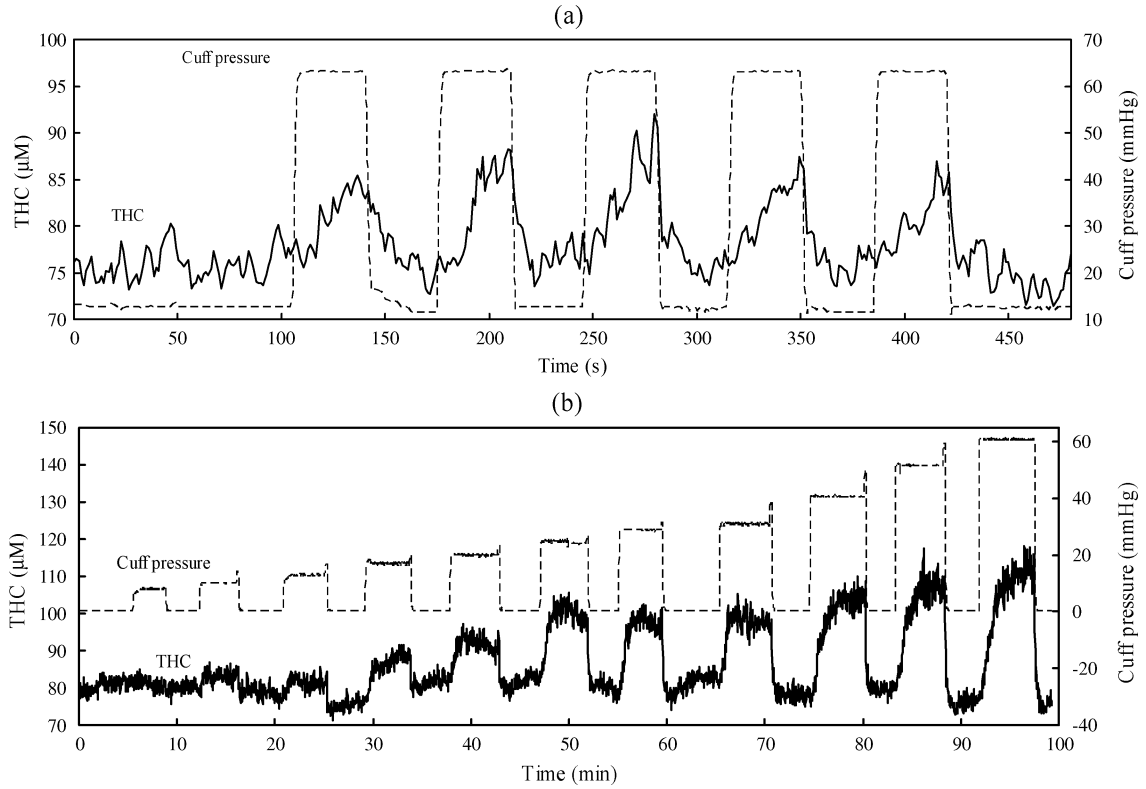

Fig. 4. The dashed lines represent the cuff pressure applied to the subject's upper arm during (a) protocol 1 and (b) protocol 2 as measured by a digital manometer. The continuous lines are the time traces of the THC measured with near-infrared spectroscopy on the subject's forearm (brachioradialis muscle).

D. Measurement Protocols

Six healthy human subjects participated in the experiments, three males and three females, 35 years of average age (range: 26–52 years; standard deviation: 9.3 years). All six subjects performed both protocols described below. The first protocol, aimed at studying the temporal features of the hemodynamic changes in the forearm in response to a 60 mmHg cuff pressure to the upper arm, was performed to validate the model predictions for the time dependence of blood volume. The second protocol, involving the application of increasing cuff pressure values, was performed to validate the model predictions for the dependence on the cuff pressure of 1) the asymptotic changes in THC and StO_2 and 2) the initial rate of increase of THC. During the experiments, the subject's arms were rested at the heart level, while the subject was comfortably sitting on an armchair. In some subjects, we repeated one or both protocols two or three times to test reproducibility and we always found the results to be reproducible. The experimental protocols and procedures were approved by the Tufts University Institutional Review Board, and a signed informed consent was obtained from all subjects prior to the experiments.

1) Protocol 1: Hemodynamic Response to Venous Occlusion: The first protocol consisted of an initial baseline acquisition (about 2 min) and the repetition for five times of the following set of procedures: 1) fast cuff inflation to 60 mmHg (inflation rate: ∼20 mmHg/s); 2) maintaining the cuff pressure at 60 mmHg for 40 s; 3) fast deflation of the cuff (deflation rate: ∼30 mmHg/s); 4) maintaining the cuff deflated for 30 s. A cuff pressure value of 60 mmHg achieves venous occlusion in the upper arm. The time-dependence of the cuff pressure for protocol 1 is shown by the dashed line of Fig. 4(a) for the measurement on patient number 2.

2) Protocol 2: Effect of Cuff Pressure: The second protocol consisted of a few minutes of baseline acquisition and the repetition of the following four steps for 11 different values of cuff pressure: 1) fast cuff inflation (∼20 mmHg/s) to a given pressure value; 2) maintaining the cuff pressure for 3–5 min until the THC reached steady-state (which typically occurred after ∼2–3 min); 3) quickly deflate the cuff (typically over 1–2 s). The cuff was inflated to a different value for each of the 11 repetitions of the above steps, with a range of values of 10–60 mmHg. The time-dependence of the cuff pressure for protocol 2 is shown by the dashed line of Fig. 4(b) for the measurement on patient number 2.

III. Results

A. Protocol 1: Hemodynamic Response to Venous Occlusion

Fig. 4(a) shows a typical response of the THC measured with near-infrared spectroscopy on the subject's forearm during protocol 1 [periodic inflation and deflation of the pneumatic cuff at the upper arm as indicated by the dashed line of Fig. 4(a)]. Fig. 4(a) reports the data measured on subject 2. The THC increases during the time that the cuff is inflated because of the accumulation of blood in the forearm induced by the venous occlusion in the upper arm. The folding average over the five repetitions of the inflation/deflation procedures is reported in Fig. 5 for all six subjects examined and shows the level of inter-subject reproducibility of the results. The grand average of the THC data

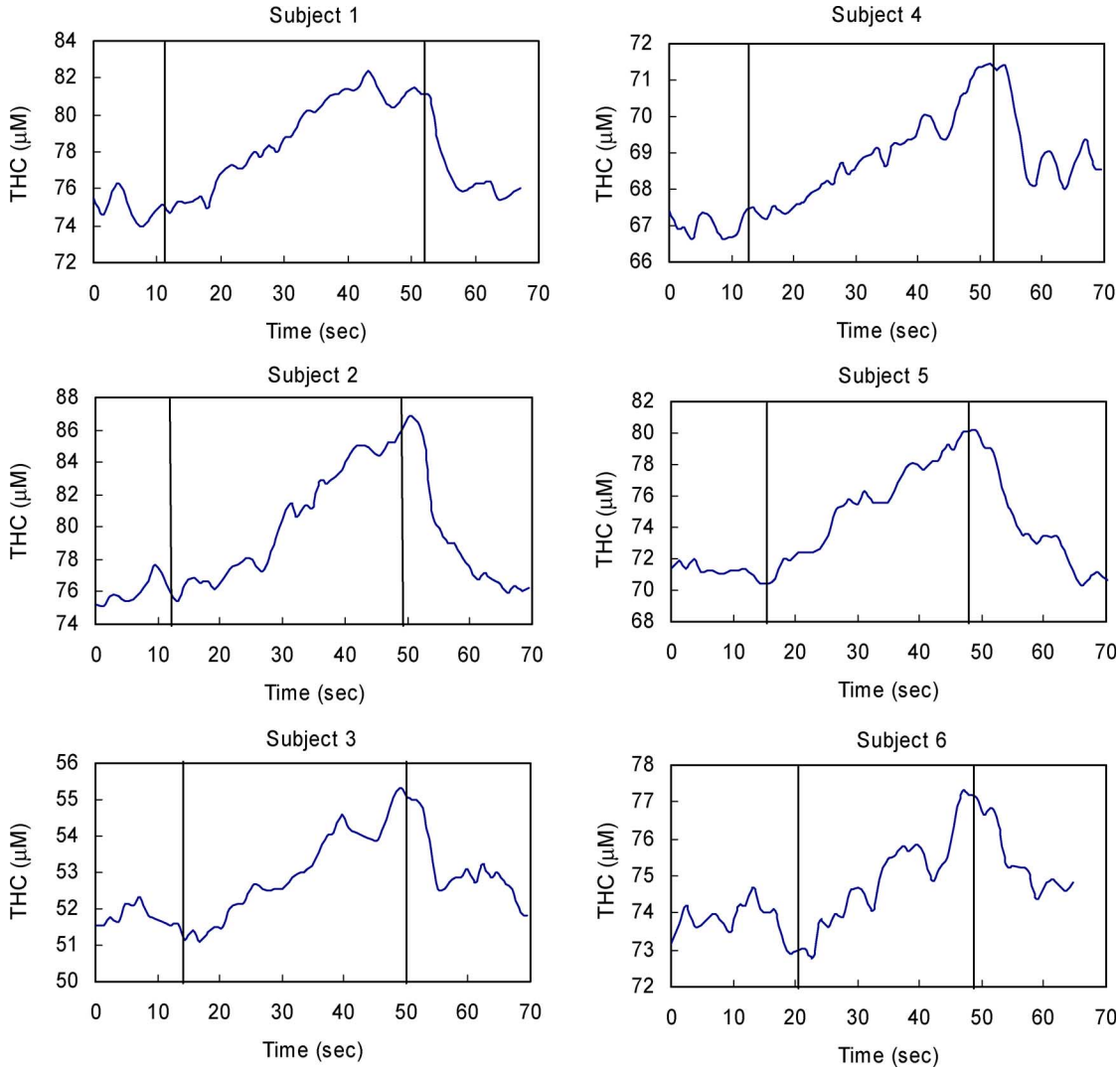

Fig. 5. THC measured in the forearm (brachioradialis muscle) of each of the six subjects examined during protocol 1. The vertical lines indicate the start and the end of the venous occlusion by applying a cuff pressure of 60 mmHg around the upper arm.

($\langle \mathrm{THC} \rangle$) across all subjects is shown in Fig. 6 (open circles). The experimental data of $\langle \mathrm{THC} \rangle$ is compared with model fits for the cases of "small" V_{ext} (i.e., $V_{\mathrm{ext}} < V_{\mathrm{crit}}$) and "large" V_{ext} (i.e., $V_{\mathrm{ext}} \geq V_{\mathrm{crit}}$) of the voltage-source/diode circuit model of Fig. 1(b). For this comparison, we have used the expressions for $v_c(t)$ that are reported in Tables II and III. The capacitor voltage v_c is proportional to the capacitor charge, which describes the blood volume in this model. To fit the model to our data, we first computed the resting level of $\langle \mathrm{THC} \rangle$ as the mean of the experimental data before the vascular occlusion. Next we fit the post-occlusion recovery phase of the data with its model equation by varying two parameters: 1) the time constant; 2) the value of $\langle \mathrm{THC} \rangle$ at the time of cuff pressure release, computing an error surface (mean-squared error) over that 2-D space, and finding the coordinates of the minimum error. The rising portion of the response during the occlusion is described by the same time constant in the case of the single-time-constant, "small" step model, and this model fit is shown by the thick dotted line of Fig. 6. For the two-time-constant, "large" step model, the rising phase of the response was fit again by the 2-D least squares procedure described above, where the fitting parameters are the time constant and the asymptotic, steady-state value of $\langle \mathrm{THC} \rangle$ during occlusion. This "large" step model response is shown in Fig. 6 by the thin solid line.

This result clearly shows that two distinct time constants are necessary to describe the experimental data. This indicates that the value of V_{ext} that corresponds to a cuff pressure of 60 mmHg is greater than V_{crit}. Specifically, τ_1 (the time constant following cuff release) was found to be $\sim$5 s while τ_2 (the initial time constant during cuff inflation) was found to be $\sim$73 s. These are in close agreement with the values computed from nominal values of resistance and compliance that appear in Table I for the variable resistance model ($\tau_1 = 5$ s and $\tau_2 = 79$ s.)

B. Protocol 2: Effect of Cuff Pressure

Fig. 4(b) reports the THC data collected with NIRS during protocol 2. In this case, the pressure of cuff inflation was varied for each repetition and kept for a sufficiently long time to allow the THC to reach steady-state. The steady-state values of $\Delta\mathrm{THC}$ and $\Delta\mathrm{StO_2}$ are predicted by the voltage source

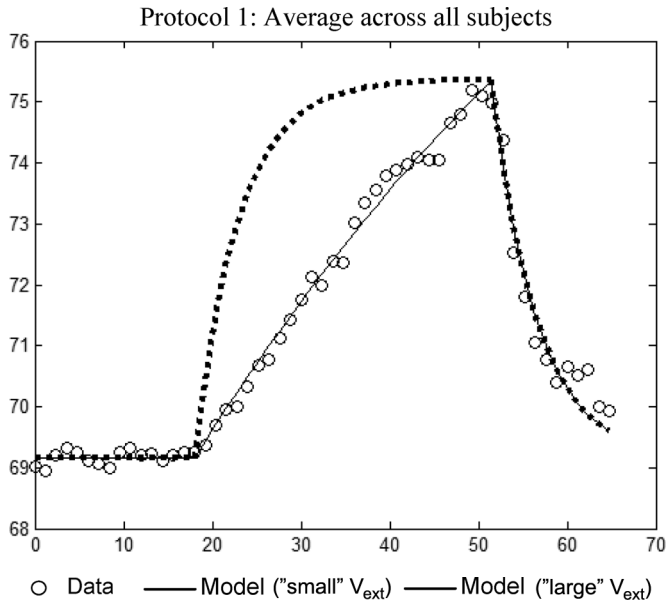

Fig. 6. Average across all six subjects of the temporal response of THC to venous occlusion. The symbols represent the experimental data, the dashed line represents the one-time-constant, voltage source model ("small" $V_{\rm ext}$, where the diode is always conducting), and the solid line represents the two-time-constant, voltage source model ("large" $V_{\rm ext}$, where the diode is nonconducting during the initial period of occlusion).

model of Fig. 1(b) to be linearly dependent on the cuff pressure. In fact, after defining $A = (V_a - V_v)/(R_a + R_v)$ and $B = 1/(R_a + R_v)$, the limiting expressions for steady-state (ss) v_c (which models THC) and i_a (which models $\mathrm{StO_2}$) during occlusion are given by $v_c^{(ss)} = V_a - AR_a + BR_aV_{\rm ext}$, and $i_a^{(ss)} = A - BV_{\rm ext}$, respectively. Fig. 7(a) and (b) reports the experimental results for the dependencies of $\langle\Delta\mathrm{THC}\rangle$ and $\langle\Delta\mathrm{StO_2}\rangle$ (averaged across all subjects). The linear dependence of the limiting values of v_c and i_a as a function of external voltage, as well as the fact that the slope of v_c is positive and the slope of i_a is negative, are consistent with the experimental dependencies of $\langle\Delta\mathrm{THC}\rangle$ and $\langle\Delta\mathrm{StO_2}\rangle$ on the cuff pressure.

The initial rate of increase of THC during venous occlusion ($d\mathrm{THC}/dt$ at $t = t_1^+$ in our model) has been used to measure the blood flow in skeletal muscle using NIRS [11], [14]. For blood flow measurements, the time derivative of THC is divided by the hemoglobin concentration in blood. Our model predicts that such initial rate of increase of THC is linear with cuff pressure for the case $V_{\rm ext} < V_{\rm crit}$ but is independent of cuff pressure for the case $V_{\rm ext} \geq V_{\rm crit}$. In fact, for $V_{\rm ext} < V_{\rm crit}$, $d\mathrm{THC}/\mathrm{dt}(\mathrm{t}_1^+) = V_{\rm ext}/(R_vC)$ whereas for $V_{\rm ext} \geq V_{\rm crit}$, $d\mathrm{THC}/\mathrm{dt}(\mathrm{t}_1^+) = (V_a - V_v)/[(R_a + R_v)C]$. Because of the continuity of v_c as a function of $V_{\rm ext}$, when $V_{\rm ext}$ assumes the value of $V_{\rm crit}$ the expressions for $d\mathrm{THC}/\mathrm{dt}(\mathrm{t}_1^+)$ in the two cases coincide. Fig. 7(c) shows the values of blood flow (BF) computed from the experimental data using the equation $\mathrm{BF} = (1/K)(d\mathrm{THC}/dt)|_{\max}$, where K is the concentration of hemoglobin in blood for which we have assumed a typical value of 2.3 mM, and we have used the maximum time derivative of THC during the first 10 s of occlusion [25]. The experimental results of Fig. 7(c) are consistent with the model prediction of a linear

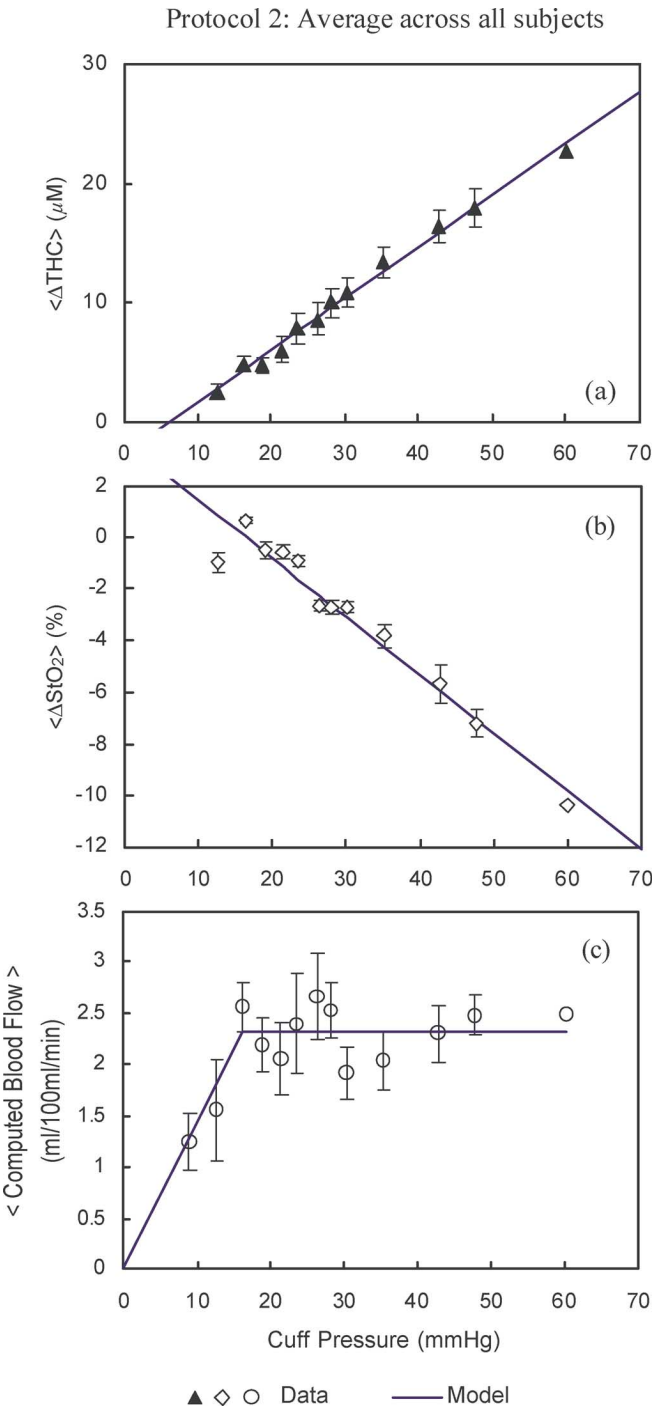

Fig. 7. Average across all six subjects of the cuff pressure dependence for the changes induced by occlusion in (a) THC ($\Delta\mathrm{THC}$), (b) tissue saturation ($\Delta\mathrm{StO_2}$), and (c) blood flow computed by the initial rate of increase of THC. The symbols represent the experimental data, whereas the lines represent the qualitative model predictions, namely a linear increase in (a) $\Delta\mathrm{THC}$, (b) a linear decrease in $\Delta\mathrm{StO_2}$ and (c) a biphasic behavior of the early slope of THC that linearly increases at low pressures while it becomes a constant at higher pressures.

behavior of the initial slope of THC as a function of cuff pressure (at small cuff pressures) and a constant value of the initial slope of THC for cuff pressures greater than a critical value, which for our data is ∼18 mmHg.

IV. Discussion

Our model of hemodynamic response to venous occlusion provides a tool to extract physiological information such as vascular resistance, compliance, blood flow and rate of oxygen metabolism from noninvasively acquired NIRS signals. While broad estimates of these physiological variables can be found in the literature, values vary widely among individuals and even within individuals as functions of activity level, age or disease state. The model provides a way to estimate specific values for a given patient. Using the voltage source model of Fig. 1(b) and the grand average of THC signals from protocol 1, it is possible to determine the relative values of R_a and R_v from the relative values of the time constants τ_1 and τ_2. Furthermore, by making repeated measures over a period of time, it might be possible to study changes in vascular compliance with aging. For example, if both time constants increase but their ratio remains unchanged, an increase in vascular compliance might be suspected. The model could also be used for testing the efficacy of vasoactive drugs, because these drugs preferentially affect the resistance vessels (the arterioles), thus causing a big change in R_a and minimally affecting R_v or C. This would manifest itself as a change in the ratio of R_a to R_v.

The diode in the model of Fig. 1(b) accounts for the existence of a critical pressure for complete venous occlusion, as previously observed experimentally in the human leg at a pressure value between 30 and 45 mmHg [14]. In this work, which involves venous occlusion in the human arm, we have found a value of about 18 mmHg for the critical pressure. By extrapolating the data for $\langle \Delta \mathrm{THC} \rangle$ of Fig. 7(a) to $\langle \Delta \mathrm{THC} \rangle = 0$, we observe a threshold pressure value of $\sim$5 mmHg to induce blood accumulation in the forearm, which is lower than the reported value of $\sim$30 mmHg for the human leg [14]. We believe that the lower values of the threshold and critical cuff pressures in the forearm with respect to the leg result from the larger size of the leg muscles. At cuff pressures greater than the critical pressure of $\sim$18 mmHg, the initial rate of increase of THC during occlusion becomes a constant [see Fig. 7(c)]. Such initial rate of increase in THC is the key parameter used for the measurement of blood flow in the venous occlusion protocol [11]. Furthermore, for cuff pressure values around the critical pressure, we have reproducibly observed in all subjects a plateau in the pressure dependence of $\Delta \mathrm{THC}$ [at 15–20 mmHg in Fig. 7(a)].

The model presented here is specifically aimed at describing the hemodynamic response to venous occlusion in a human limb. This model cannot be directly applied to the case of arterial occlusion since once a complete venous occlusion is achieved (i.e. $i_v = 0$), the arterial branch and its current i_a do not depend any more on the external pressure (described by the variable resistor in the circuit of Fig. 1(a) and by v_{ext} in the circuit of Fig. 1(b). Another limitation of the model is the use of a fixed capacitor to describe the venous compliance. Veins are known to decrease in compliance at high transmural pressures, as occur during downstream occlusion. This effect could be significant for the "large" cuff pressure steps used in our experimental protocol 1.

A mathematical model to describe reactive hyperemia following arterial occlusion has recently been reported and applied to the analysis of laser Doppler perfusion monitoring data [8]. The model of [8] focuses on the description of the blood flow in extremities in response to arterial occlusion, and presents some similarities with our model in the fact that the arterial and capillary systems are described by a similar network of resistors and capacitors. However, in the model presented here, we have aimed at describing both the blood volume accumulation during venous occlusion and the postocclusive hemodynamic response. To achieve this objective, we have modeled the effect of the externally applied pressure either with a variable resistor Fig. 1(a) or with a voltage source in series with a nonlinear circuit element (diode) to impose the unidirectional flow of current throughout the circuit Fig. 1(b). By introducing an external voltage source to model the cuff pressure, the circuit model of Fig. 1(b) lends itself to the analysis of more general time-dependent patterns of venous occlusion than the square wave external voltage considered here (Fig. 2).

V. Conclusion

We have presented a mathematical model represented in terms of an electrical circuit (featuring either a variable resistor or a voltage source/diode combination) to describe the hemodynamic response in a human limb during and following venous occlusion. We have found a good qualitative agreement between the model predictions and measurements of concentration and oxygen saturation of hemoglobin performed with near-infrared spectroscopy on the forearm of human volunteers. Because venous occlusion protocols have the potential to provide valuable physiological information (for example on blood flow, metabolic rate of oxygen, vascular compliance and resistance, etc.), this model can help design experimental protocols and interpret experimental data aimed at providing diagnostic/functional information.

Appendix
Analysis of the Voltage-Source/Diode Circuit Model for a Rectangular External Voltage

The circuit of Fig. 1(b) can be analyzed using standard circuit theory approaches. Here, we report the analytical solutions for i_a, i_v, and v_c in response to a rectangular external voltage expressed as $v_{\mathrm{ext}} = V_{\mathrm{ext}}[\theta(t-t_1) - \theta(t-t_2)]$, where V_{ext} is the amplitude of the rectangular wave, $\theta(x)$ is the step function defined as $\theta(x) = 0$ if $x < 0$ and $\theta(x) = 1$ if $x \leq 0$, and (t_1, t_2) is the time interval during which the external voltage is applied. Two cases must be considered depending on whether the external voltage is less than or greater than the critical voltage V_{crit} that switches the diode from a forward to a reverse polarization. In the first case of $V_{\mathrm{ext}} < V_{\mathrm{crit}}$ the ideal diode is always conducting and the circuit is characterized by only one time constant τ_1. In the second case, the application of a $V_{\mathrm{ext}} \geq V_{\mathrm{crit}}$ causes the diode to be initially reverse-biased, thus introducing a temporary second circuit time constant τ_2. We also set an upper limit of $V_a - V_v$ for V_{ext} consistent with the fact that here we consider a model for venous occlusion that involves external pressures that are less than the difference between arterial and venous pressure. To simplify the analytical expressions, we define the following parameters:

$V_{\text{crit}} = (V_a - V_v)R_v/(R_a + R_v)$ Critical value of V_{ext} for reverse bias of the diode D.

$I_a^{(\text{rest})} = I_v^{(\text{rest})} = (V_a - V_v)/(R_a + R_v)$ Arterial and venous currents at rest (i.e., at times $t < t_1$ and $t \to \infty$).

$I_a^{(\text{occl})} = I_v^{(\text{occl})} = V_a - V_v - V_{\text{ext}}/(R_a + R_v)$ Asymptotic values for the arterial and venous currents (blood flow) induced by V_{ext}.

A. Case of "Small" External Voltage $V_{\text{ext}} < V_{\text{crit}}$

In this case, the circuit is characterized by a single time constant $\tau_1 = R_a R_v/(R_a + R_v)C$. The analytical expressions for the arterial current, venous current, and capacitor voltage for this case are reported in Table II.

B. Case of "Large" External Voltage $V_{\text{ext}} \geq V_{\text{crit}}$

In this case, in addition to the time constant $\tau_1 = R_a R_v/(R_a + R_v)C$, the circuit is characterized by a second time constant $\tau_2 = R_a C > \tau_1$ at times $t_1 \leq t < t^*$. The time t^* is the time at which the capacitor voltage $v_c(t^*)$ equals $V_{\text{ext}} + V_v$ and can be expressed as $t^* = t_1 + \tau_2 \ln(I_a^{(\text{rest})} R_a/(I_a^{(\text{occl})}(R_a + R_v)))$. The analytical expressions for the arterial current, venous current, and capacitor voltage for this case are reported in Table III.

ACKNOWLEDGMENT

The authors would like to thank M. Ferrari and V. Quaresima for useful discussions.

REFERENCES

[1] N. Westerhof, G. Elzinga, and P. Sipkema, "An artificial arterial system for pumping hearts," *J. Appl. Physiol.*, vol. 31, pp. 776–781, 1971.

[2] N. Stergiopulos, B. Westerhof, and N. Westerhof, "Evaluation of methods for the estimation of total arterial compliance," *Am. J. Physiol. Heart Circ. Physiol.*, vol. 276, pp. H81–H88, 1999.

[3] M. S. Olufsen, A. Nadim, and L. Lipsitz, "Dynamics of cerebral blood flow regulation explained using a lumped parameter model," *Am. J. Physiol. Regul. Integr. Comp. Physiol.*, vol. 282, pp. R611–R622, 2002.

[4] S. L. Voytik, C. F. Babbs, and S. F. Badylak, "Simple electrical model of the circulation to explore design parameters for a skeletal muscle ventricle," *J. Heart Transplantation*, vol. 9, pp. 160–174, 1990.

[5] C. F. Babbs, J. C. Weaver, S. H. Ralston, and L. A. Geddes, "Cardiac, thoracic, and abdominal pump mechanisms in cardiopulmonary resuscitation: studies in an electrical model of the circulation," *Am. J. Emerg. Med.*, vol. 2, pp. 299–308, 1984.

[6] R. Olmi, S. Andreoli, M. Bini, P. Feroldi, and L. Spiazzi, "An electrical model of biological tissues undergoing hyperaemia," *Phys. Med. Biol.*, vol. 43, pp. 3405–341, 1998.

[7] A. Sainz, J. Cabau, and V. C. Roberts, "Deceleration vs. acceleration: a haemodynamic parameter in the assessment of vascular reactivity: A preliminary study," *Med. Eng. Phy.*, vol. 17, pp. 91–95, 1995.

[8] F. F. M. de Mul, F. Morales, A. J. Smit, and R. Graaff, "A model for post-occlusive reactive hyperemia as measured with laser-Doppler perfusion monitoring," *IEEE Trans. Biomed. Eng.*, vol. 52, no. 2, pp. 184–190, Feb. 2005.

[9] N. B. Hampson and C. A. Piantadosi, "Near infrared monitoring of human skeletal muscle oxygenation during forearm ischemia," *J. Appl. Physiol.*, vol. 64, no. 6, pp. 2449–2457, 1988.

[10] M. C. P. van Beekvelt, W. N. J. M. Colier, B. G. M. van Engelen, M. T. E. Hopman, R. A. Wevers, and B. Oeseburg, "Validation of measurement protocols to assess oxygen consumption and blood flow in the human forearm by near infrared spectroscopy," *Proc. SPIE*, vol. 3194, pp. 133–144, 1998.

[11] R. A. de Blasi, M. Ferrari, A. Natali, G. Conti, A. Mega, and A. Gasparetto, "Noninvasive measurement of forearm blood flow and oxygen consumption by near-infrared spectroscopy," *Appl. Physiol.*, vol. 76, no. 3, pp. 1388–1393, 1994.

[12] C. W. Yoxall and A. M. Weindling, "Measurement of venous oxyhaemoglobin saturation in the adult human forearm by near infrared spectroscopy with venous occlusion," *Med. Biol. Eng. Comput.*, vol. 35, pp. 331–336, 1997.

[13] M. Nitzan, A. Babchenko, B. Khanokh, and H. Taitelbaum, "Measurement of oxygen saturation in venous blood by dynamic near infrared spectroscopy," *J. Biomed. Opt.*, vol. 5, pp. 155–162, 2000.

[14] C. Casavola, L. A. Paunescu, S. Fantini, and E. Gratton, "Blood flow and oxygen consumption with near-infrared spectroscopy and venous occlusion: spatial maps and the effect of time and pressure of inflation," *J. Biomed. Opt.*, vol. 5, pp. 269–276, 2000.

[15] J. J. Smith and J. P. Kampine, *Circulatory Physiology*, 3rd ed. Baltimore, MD, USA: Williams & Wilkins, 1990.

[16] G. Dai, J. P. Gertler, and R. D. Kamm, "The effects of external compression on venous blood in the lower leg," *J. Biomech. Eng.*, vol. 121, pp. 557–564, 1999.

[17] A. H. Moreno, A. I. Katz, L. D. Gold, and R. V. Reddy, "Mechanics of distension of dog veins and other very thin-walled tubular structures," *Circ. Res.*, vol. 27, pp. 1069–1080, 1970.

[18] S. Ramanujan, "Modular equations and approximations to," *Quart. J. Pure Appl. Math.*, vol. 45, pp. 350–372, 1913.

[19] J. D. Hoffman, *Numerical Methods for Engineers and Scientists*, 2nd ed. New York: Marcel Decker, 2001.

[20] J. P. Holt, "Flow of liquids through "collapsible" tubes," *Circ. Res.*, vol. 7, pp. 342–353, 1959.

[21] D. H. Wiener, C. I. Fink, J. Maris, R. A. Jones, B. Chance, and J. R. Wilson, "Abnormal skeletal muscle bioenergetics during exercise in patients with heart failure: role of reduced muscle blood flow," *Circulation*, vol. 73, pp. 1127–1136, 1986.

[22] J. McLeod, "PHYSBE . . .a physiological simulation benchmark experiment," *Simulation*, vol. 7, pp. 324–329, 1966.

[23] S. Fantini, M. A. Franceschini, J. B. Fishkin, B. Barbieri, and E. Gratton, "Quantitative determination of the absorption spectra of chromophores in strongly scattering media: a light-emitting-diode based technique," *Appl. Opt.*, vol. 33, pp. 5204–5213, 1994.

[24] S. Fantini, "A haemodynamic model for the physiological interpretation of *in vivo* measurements of the concentration and oxygen saturation of haemoglobin," *Phys. Med. Biol.*, vol. 47, pp. N249–N257, 2002.

[25] V. Quaresima, M. Ferrari, M. A. Franceschini, M. L. Hoimes, and S. Fantini, "Spatial distribution of vastus lateralis blood flow and oxyhemoglobin saturation measured at the end of isometric quadriceps contraction by multichannel near-infrared spectroscopy," *J. Biomed. Opt.*, vol. 9, pp. 413–420, 2004.

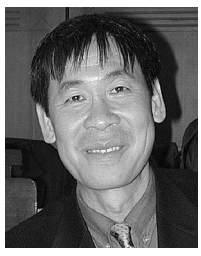

Toi Van Vo received the Ph.D. degree from the Swiss Federal Institute of Technology, Lausanne, Switzerland.

He has been with Tufts University, Medford, MA, since 1984. His research interests include design and applications of medical instrumentation, human visual system and ophthalmology, effects of electromagnetic fields in human adult stem cells, and information technology in healthcare. He co-founded the Vietnamese North American University Professor Network to promote interaction among university professors of Vietnamese extraction in the U.S. and Canada. He strives to promote research, education, and entrepreneurship of biomedical engineering in Vietnam, and cooperation between the U.S. and Vietnamese scientific communities in this field.

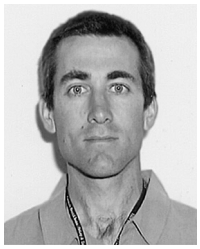

Peter E. Hammer received the B.S. degree in mechanical engineering from the University of New Hampshire, Durham, in 1988 and the M.S. degree in biomedical engineering from Boston University, Boston, MA, in 1997. He is currently working toward the Ph.D. degree in biomedical engineering from Tufts University, Medford, MA.

He worked as a Manufacturing Engineer in the electronics industry for five years before returning to school to study biomedical engineering. Since 1995, he has worked as a Research Engineer at Children's Hospital, Boston, on topics including heart rate variability analysis, mathematical modeling of baroreflex control, cardiac arrhythmia mapping, and computational modeling of mitral valve mechanics.

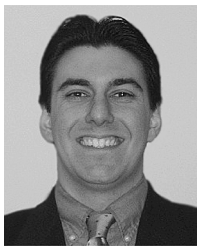

Matthew L. Hoimes is originally from Stony Brook, NY. He attended the combined engineering and medical degree program at Tufts University, Medford, MA. He received the B.S. degree in electrical engineering, the M.S. degree in biomedical engineering, and the M.D. degree from Tufts University in 2005.

He completed his internship at Newton Wellesley Hospital. He is currently completing residency training in radiology at Tufts-New England Medical Center, Boston. His research and career goals are concentrated on collaboration between engineering and medical fields to help advance medical imaging technology.

Dr. Hoimes was recognized with the surgical house-officer of the year award.

Shalini Nadgir received the B.E. degree in medical electronics from the B.M.S. College of Engineering, Bangalore University, Bangalore, India, in 1998 and the M.S. degree in biomedical engineering from Tufts University, Medford, MA, in 2003. Her master's project was on "Non-invasive measurement of oxygenation changes using Near Infrared Spectroscopy (NIRS) during venous occlusion of the forearm." Thesis submitted: "Non-invasive measurement of cerebral oxygenation changes using NIRS during electro-convulsive therapy."

She worked part-time as Research Assistant at Tufts University. She is currently a Research Technologist involved in taking measurements on cerebral oxygenation changes of newborns using NIRS at the Massachusetts General Hospital (MGH), Boston.

Sergio Fantini received the Ph.D. degree in physics from the University of Florence, Florence, Italy, in 1992.

After postdoctoral and faculty appointments in the Physics Department at the University of Illinois at Urbana-Champaign from 1993 to 1999, he joined Tufts University, Medford, MA, where he is currently Professor of Biomedical Engineering and Associate Dean for Graduate Education in the School of Engineering. His research interests are in diffuse optical imaging and spectroscopy of biological tissues, with applications in areas such as tissue oximetry, breast cancer detection, and functional imaging of the brain.